Polymer Chemistry

Accepted Manuscript

ROYAL SOCIETY OF CHEMISTRY

www.rsc.org/polymers

Rhodamine based pH-sensitive "intelligent" polymer as lysosome targeting probes and their imaging application *in vivo*

Kang-Kang Yu,[a] Kun Li,*[a,b] Ji-Ting Hou,[a] Jin Yang,[a] Yong-Mei Xie*[b] and Xiao-Qi Yu *[a]

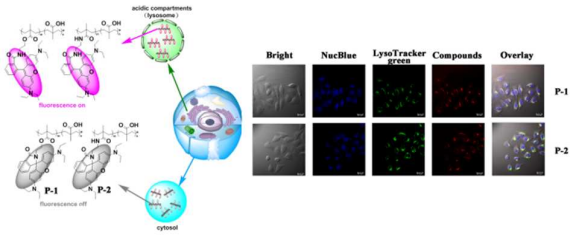

Two rhodamine-based polymers (**P-1** and **P-2**) were prepared via atom transfer radical polymerization (ATRP), which could be served as lysosome targeting probes with good pH sensitivity. Moreover, fluorescence imaging of nude mice of **P-1** and **P-2** displayed a chance for the visualization of cancerous tissue in *vivo* by sensing the tumor acidic microenvironments.

Cite this: DOI: 10.1039/c0xx00000x

www.rsc.org/xxxxxx

ARTICLE TYPE

Rhodamine based pH-sensitive "intelligent" polymer as lysosome targeting probes and their imaging application *in vivo*†

Kang-Kang Yu,[a] Kun Li,*[a,b] Ji-Ting Hou,[a] Jin Yang,[a] Yong-Mei Xie*[b] and Xiao-Qi Yu *[a]

Received (in XXX, XXX) Xth XXXXXXXXX 20XX, Accepted Xth XXXXXXXXX 20XX

DOI: 10.1039/b000000x

Two rhodamine-based polymers (**P-1** and **P-2**) were prepared *via* a free radical polymerization, which could be served as lysosome targeting probes with prominent pH sensitivity. The polymers exhibited suitable water solubility and the content of rhodamine in them were determined through ^{1}H NMR and ultraviolet-visible absorption spectra. Both **P-1** and **P-2** have excellent selectivity, membrane permeability and low cytotoxicity. Confocal microscopy was used to investigate the intracellular distribution of lysosomes and visualizing pH-responsive changes in the liver of zebrafish. Moreover, fluorescence imaging of nude mice of **P-1** and **P-2** displayed a chance for the visualization of cancerous tissue *in vivo* by sensing the tumor acidic microenvironments.

Introduction

For the highly compartmentalized eukaryotic cells, intracellular pH is a crucial physiologic parameter: almost all of the proteins need appropriate pH to maintain their structure and function, the charge of biological surfaces is dictated by protonation-deprotonation events[1], and intracellular pH is closely related to ion transport, multidrug resistance and muscle contraction[2-5]. Compared with the nearly neutral cytoplasma (pH 7.2)[1,6-7], there are some acidic compartments (pH 4.5-6.0)[8-11], including endosomes, lysosomes and autophagosome[12], which contain approximately 50 different degradative enzymes that are active at acidic pH (~ 5)[13] and have great connections with cell proliferation, apoptosis and endocytosis[14]. Considering that abnormal pH values in living cells and organisms is often associated with dysfunctions and pathological processes[15], developing intracellular pH indicator for providing significant information of physiological and pathological processes have attracted increasing attention. In addition, dysregulated pH has been reported as one of the characteristics of cancer[16]: under physiological conditions, the pH of normal tissue is about 7.4, but tumor tissue *in vivo* is more acidic (pH 6.2-6.9)[17], which indicated that the precise sensing of pH variations is also quite crucial for the diagnosis and treatment of cancer.

Many methods have been used for detecting the variation of pH including microelectrodes, nuclear magnetic, absorption and fluorescence spectroscopy[18]. Among these methods, fluorescence detector have been intensively studied because of its operational simplicity, fast response time, non-invasive, low cost, high selectivity, real time sensing and easily miniaturized, moreover its applications in bioimaging, environmental analysis and the visual diagnosis and treatment of disease still has much evolvable space[19].

Over the past decades, several small molecular fluorescent pH sensors have been reported[20-28]. Nevertheless, small molecular sensors can suffer from leakage from cells, usually have poor control over subcellular targeting and might cause non-negligible bio-toxicity[29]. To overcome this problem, a number of polymer-based fluorescent probes were explored and they exhibited notably higher sensitivity because of the polymer amplification effect which could afford fast charge and energy migration along the backbone of polymer[30-31]. Recently, researchers have developed several pH-responsive materials. In 2010, Beltram and Wei reported a subcellular targeting dendrimer-based fluorescent pH sensors[32] and a Dextran based pH-activated near-infrared fluorescence nanoprobe, respectively[33]. Ma has developed a pH sensor based on carbon nanodots in 2012[34]. Not long ago, Shi reported a pH-triggered nanoprobe based on PET mechanism[35]. Although these pH-triggered materials are sensitive and can be used for cells imaging, the preparations are a little complicated, the grafting degree of fluorophore is instable and cytotoxicity of them are not satisfying. Recently, Han's group presented a rhodamine-deoxylactam functionalized poly[styrene-alter-(maleic acid)]s as lysosome activatable probes[36] and a targetable acid-responsive micellar system consisting of cores of rhodamine-sultam (RST) and glycosylated poly[styrene-alter-(maleic acid)][37], but the instability of the grafting degree is still exist due to the polymerization method they explored. Inspired by Han's work, we want to develop a novel polymeric fluorescent pH indicator with low background interference and highly sensitivity, which could be synthesized with stable grafting degree by simple method and could be further apply to not only the imaging of subcellular acidic organelles (especially lysosome) but also some other applications *in vivo* (zebrafish , mice).

As we know, free radical polymerization is a key synthesis route for obtaining a wide variety of different polymers and material composites by introducing different monomers[38-40]. We decide to prepare the degradable polymers with suitable water

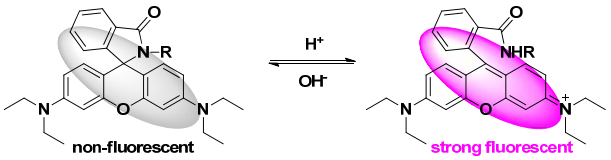

Scheme 1 Mechanism of spirolactam ring-opening

solubility *via* free radical polymerization. In Addition, rhodamine, as one of the most widely used fluorescent dyes, exhibits excellent photostability, photophysical properties and also has proper water solubility (these properties make rhodamine dervatives can be used for fluorescence imaging *in vivo*)[41-47], More importantly, the spirolactam structure of rhodamine derivatives is very sensitive to the pH variations: the spirolactam remains closed and non-fluorescent in the basic or neutral environment; whereas acidic condition leads to the ring-opening of spirolactam and the rhodamine derivatives exhibit strong emission and a pink color (Scheme 1).

Contrasting with the recent specific lysosomal probes and the commercial LysoTracker indicators, which are slightly alkaline that selectively concentrate in acidic compartments upon protonation[13,48-50]. Culture cells with these probes can induce an increase of pH value in the acidic compartments, take the specific lysosomal group--morpholine for example, the inadequate fluorescence quenching of the PET mechanism often lead to high nonspecific background fluorescence signals inside cells, however the H^+ triggered ring-opening mechanism of rhodamine effectively preventing the interference of background fluorescence[51]. Herein we decided to utilize rhodamine derivatives as pH-sensitive monomers and prepare a polymeric fluorescence sensing platform *via* free radical polymerization, aiming at developing a highly sensitive and biocompatible pH sensor for intracellular acidic organelles imaging and with the potential to visualize tumors by sensing tumor.

2. Experimental

2.1 Reagents and chemicals

Rhodamine B , 2-aminoethanol , ethanediamine , triethylamine , methacryloyl chloride, methacrylic acid, 2,2'-azobisisobutyronitrile (AIBN), cyclohexanone and ether were of analytical grade and used without further purification, unless otherwise noted, materials were obtained from commercial suppliers. Methanol, ethanol and dichloromethane were dried according to the standard methods prior to use. All of the solvents were either HPLC or spectroscopic grade in the optical spectroscopic studies. Lysotracker green DND-26 and NucBlue® Live Cell Stain was purchased from Invitrogen.

Birtton-Robison (B-R) buffer solutions consist of 40 mM boric acid, 40 mM phodphoric acid, 40 mM acetic acid and 20 mM sodium hydroxide were used for tuning pH values[52]. All samples for fluorescence experiments were performed in B-R buffer solution for 30 min before measurement.

All experiments were performed in compliance with the relevant laws and institutional guidelines. All the animal procedures were performed following the protocol approved by the Institutional Animal Care and Treatment Committee of Sichuan University (Chengdu, P.R. China). All the mice were treated humanely throughout the experimental period.

2.2 Apparatus

^{1}H NMR, ^{13}C NMR spectra were measured on a Bruker AM400 NMR spectrometer. Proton Chemical shifts of NMR spectra were given in ppm relative to internals reference TMS (1H, 0.00 ppm). All pH measurements were performed with a pH-3c digital pH-meter (Shanghai Lei Ci Device Works, Shanghai, China) with a combined glass-calomel electrode. Fluorescence emission spectra were obtained using FluoroMax-4Spectrofluorophotometer (HORIBA JobinYvon) at 298 K. Fluorescence imaging of nude mice was conducted in Bio-Real *in vivo* imaging system (Quick View 3000, Bio-Real, AUSTRIA)

2.3 Syntheses

2.3.1 Syntheses of Rh-1 and Rh-2

Rh-1: A solution of rhodamine B (2.0 g, 4.1 mmol) in absolute methanol (30 ml) and 2-aminoethanol (900 µl, 16.4 mmol) was added, the resulting mixture was heated at 80 ^{o}C for 12h. Then the mixture was cooled to room temperature and the product was separated out. After filtration, the precipitate was washed by methanol (10 ml) for several times and **Rh-1** was given as light pink solid (1.51 g, 78.6%). ^{1}H NMR (400 MHz, $CDCl_3$) δ 7.90 (dd, J = 5.6, 3.0 Hz, 1H), 7.44 (dt, J = 7.3, 3.6 Hz, 2H), 7.07 (dd, J = 5.4, 3.1 Hz, 1H), 6.47 (t, J = 12.1 Hz, 2H), 6.38 (d, J = 2.5 Hz, 2H), 6.29 (dd, J = 8.9, 2.5 Hz, 2H), 3.52 – 3.43 (m, 2H), 3.39 – 3.24 (m, 10H), 1.17 (t, J = 7.0 Hz, 12H).

Rh-2: A solution of rhodamine B (2.0 g, 4.1mmol) in absolute ethanol (30 ml) and ethane diamine (1.34 ml, 20 mmol) was added, the resulting mixture was heated at reflux 12 hours. Then the solvent was distilled in vacuo, the residue was mixed with 15 ml acetonitrile and undissolved yellowish-brown solid is the crude product. After filtration, the precipitate was separated by column chromatography to give **Rh-2** (1.99 g, 91 %). ^{1}H NMR (400 MHz, $CDCl_3$) δ 7.95 – 7.84 (m, 1H), 7.50 – 7.38 (m, 2H), 7.09 (dd, J = 5.5, 3.0 Hz, 1H), 6.43 (d, J = 8.8 Hz, 2H), 6.37 (d, J = 2.5 Hz, 2H), 6.27 (dd, J = 8.9, 2.6 Hz, 2H), 3.33 (q, J = 7.1 Hz, 8H), 3.19 (t, J = 6.6 Hz, 2H), 2.42 (t, J = 6.6 Hz, 2H), 1.16 (t, J = 7.0 Hz, 12H).

2.3.2 Syntheses of M-1and M-2

M-1: A mixture of **Rh-1** (970 mg, 2.0 mmol) and triethylamine (836 µl, 6.0 mmol) were dissolved in 30 ml anhydrous dichloromethane, and the solution was cooled with an ice bath. Methacryloyl chloride (232 µl, 2.4 mmol) was dissolved in 3 ml anhydrous dichloromethane, and then adding it to the former mixture dropwise under the ice bath. Later removed the ice bath, the mixture was stirred at room temperature for 10 hours. After evaporation, CH_2Cl_2 was added and organic layer was washed with water, dried over $MgSO_4$, and concentrated. The products were separated by column chromatography to give 920 mg **M-1** (83 %).^{1}H NMR (400 MHz, CD_3OD) δ 7.89 (dd, J = 5.8, 2.8 Hz, 1H), 7.59 – 7.48 (m, 2H), 7.06 (dd, J = 5.6, 2.4 Hz, 1H), 6.44 (d, J = 1.9 Hz, 2H), 6.40 – 6.19 (m, 4H), 6.00 (s, 1H), 5.56 (s, 1H), 3.46 (t, J = 6.0 Hz, 2H), 3.42 – 3.32 (m, 10H), 1.84 (s, 3H), 1.17 (t, J = 7.0 Hz, 12H).

M-2: A mixture of **Rh-2** (968 mg, 2.0 mmol) and triethylamine (836 µl, 6.0 mmol) were dissolved in 30 ml anhydrous dichloromethane; the solution was cooled with an ice bath. Methacryloyl chloride (232 µl, 2.4 mmol) was dissolved in

3 ml anhydrous dichloromethane, and then adding it to the former mixture dropwise under the ice bath. Later removed the ice bath, the mixture was stirred at room temperature for 10 hours. After evaporation, CH_2Cl_2 was added and organic layer was washed with water, dried over $MgSO_4$, and concentrated. The products were separated by column chromatography to give 900 mg **M-2** (81.4 %).^{1}H NMR (400 MHz, CD_3OD) δ 7.86 (dd, *J* = 5.9, 2.2 Hz, 1H), 7.61 – 7.44 (m, 2H), 7.03 (dd, *J* = 5.9, 2.0 Hz, 1H), 6.50 – 6.24 (m, 6H), 5.61 (s, 1H), 5.29 (s, 1H), 3.36 (q, *J* = 7.0 Hz, 8H), 3.27 (d, *J* = 6.3 Hz, 2H), 3.02 (t, *J* = 6.3 Hz, 2H), 1.84 (s, 3H), 1.15 (t, *J* = 7.0 Hz, 12H).

2.3.3 Syntheses of P-1 andP-2

P-1: A mixture of **M-1** (138 mg, 0.25 mmol), methacrylic acid (213 μl, 2.5 mmol) and AIBN (41 mg, 0.25 mmol) in degassed cyclohexanone/ethanol (1:1, 20 ml), the resulting mixture was stirred at 60℃ under the atmosphere of nitrogen for 12h. Then the mixture was cooled to room temperature, distilled part of the solvent in vacuo and adding ether to the mixture dropwise, the polymer was separated out. After filtration, the precipitate was washed by ether (10 ml) for several times and 312 mg **P-1** was given as pink solid.

P-2: A mixture of **M-2** (138 mg, 0.25 mmol), methacrylic acid (213 μl, 2.5 mmol) and AIBN (41 mg, 0.25 mmol) in degassed cyclohexanone/ethanol (1:1, 20 ml),the resulting mixture was stirred at 60 °C under the atmosphere of nitrogen for 12h. Then the mixture was cooled to room temperature, distilled part of the solvent in vacuo and adding ether to the mixture dropwise, the polymer was separated out. After filtration, the precipitate was washed by ether (10 ml) for several times and 221 mg **P-2** was given as pink solid.

2.4 Imaging of living cell

Hela cells were cultured in Dulbecco's modified Eagle medium (DMEM) containing 10% fetal bovine serum and 1% Antibiotic-Antimycotic at 37°C in a 5% CO_2/95% air incubator. For fluorescence imaging, cells (4×10^3/well) were passed on confocal dishes and incubated for 24h. Immediately before the staining experiment, cells were washed twice with PBS (10 mM): dish **1**incubated with 1μMLysoTracker Green and one drop NucBlue for 30 min at 37 °C; dish **2**incubated with **M-1** (5 μM), LysoTracker Green (1μM) and NucBlue (one drop) for 30 min at 37 °C; dish **3**incubated with**M-2** (5 μM), LysoTracker Green (1μM) and NucBlue (one drop) for 30 min at 37 °C; dish **4** incubated with **P-1** (25 μg/ml), LysoTracker Green (1 μM) and NucBlue (one drop) for 30 min at 37 °C; dish **5** incubated with **P-2** (25 μg/ml), LysoTracker Green (1 μM) and NucBlue (one drop) for 30 min at 37 °C. Then wash each dish with PBS (10 mM) for 3 times, and analyzed with a confocal fluorescence microscope. NucBlue(the blue emission) in 420-470 nm was collected using an excitation wavelength of 405 nm, LysoTracker Green(the green emission) in 500-540 nm was collected using an excitation wavelength of 488 nm, **M-1**, **M-2**, P-1 and **P-2** (the red emission) in 565-620 nm was collected using an excitation wavelength of 552 nm.

2.5 Zebrafish incubation and imaging

Zebrafish was kept at 28 °C and maintained at optimal breeding conditions. For mating, male and female zebrafish was maintained in one tank at 28 °C on a 12 h light/12 h dark cycle and then the spawning of eggs were triggered by giving light stimulation in the morning. Almost all the eggs were fertilized immediately. The 5-day old zebrafish was maintained in E3 embryo media (15 mM NaCl, 0.5 mM KCl, 1 mM $MgSO_4$, 1 mM $CaCl_2$, 0.15 mM KH_2PO_4, 0.05 mM Na_2HPO_4, 0.7 mM $NaHCO_3$, 10^{-5} % methylene blue; pH 7.5). The zebrafish was divided into 10 groups (each group at least contains 5 zebrafish): group **1** and **2** was only incubated in E3 media for 30 min at 28 ºC, then washed with pH 5.0 and 7.0 PBS buffer solution（10 mM），respectively. Group **3** was incubated with 100μM **M-1**in E3 media for 30 min at 28 ºC and then washed with pH 5.0 PBS (10mM) for 5 min, group **4** was also incubated with 100μM **M-1**in E3 media for 30 min at 28 ºC and then washed with pH 7.0 PBS (10mM) for 5 min, **M-2** (100μM), **P-1**(500 μg/ml) and **P-2** (500 μg/ml) repeating the steps as **M-1**. After washing with E3 media, the zebrafish was imaged by confocal laser fluorescence microscopy.

2.6 Fluorescent imaging in nude mice.

Female Balb/c-nu mice (5–6 weeks old) were purchased from Beijing HFK bioscience CO. Ltd, Beijing, China. Animal experiments were approved by the Institutional Animal Care and Treatment Committee of Sichuan University (Chengdu, China).The mice were acclimated for 1 week before the experiment.

3. Results and discussion

3.1 Synthesis and characterization of the polymers

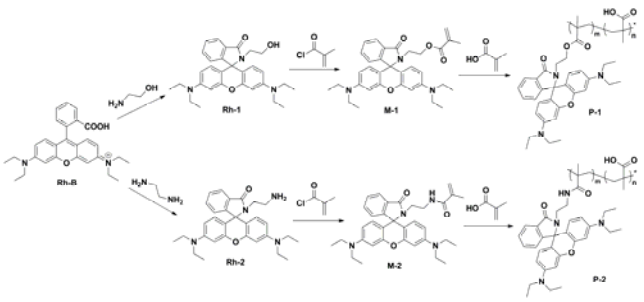

Scheme 2 Synthesis of **P-1** and **P-2**

As illustrated in Scheme 2, the monomers **M-1** and **M-2** could be easily synthesized *via* two steps with high yields. Then the polymers **P-1** and **P-2** were prepared *via* free radical polymerization reaction with methacrylic acid. **P-1** and **P-2** were characterized by ^{1}H NMR, gel permeation chromatography (GPC) as well as UV-vis absorption spectra. M_n and M_w of the two compounds were determined *via* GPC (Table S1). The difference between **P-1** and **P-2** is the linker that connected rhodamine and backbone of the polymers. Considering the different behavior of ester bond and amide, we believe they will exhibit different properties, especially inside the cells and animal models.

Subsequently, ^{1}HNMR spectrum was employed for further analysis of the polymers by contrasting with rhodamine-based monomer. As shown in Fig. 1 and Fig. 2, before the

polymerization, the characteristic peaks of hydrogen atoms of rhodamine (a, b, c, d) and olefinic bond (e, f) could be found in both ^{1}H NMR spectra of **M-1** and **M-2**, while the characteristic signal of hydrogen atoms of olefin at 6.00 ppm and 5.47 ppm for

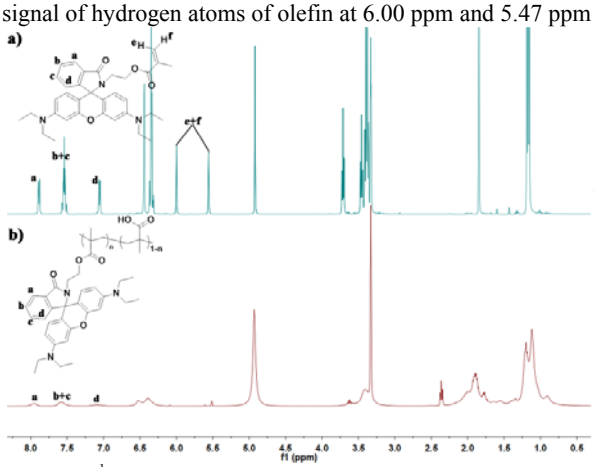

Fig. 1 ^{1}H-NMR spectra recorded for a) **M-1**, b) **P-1**. (in CD_3OD)

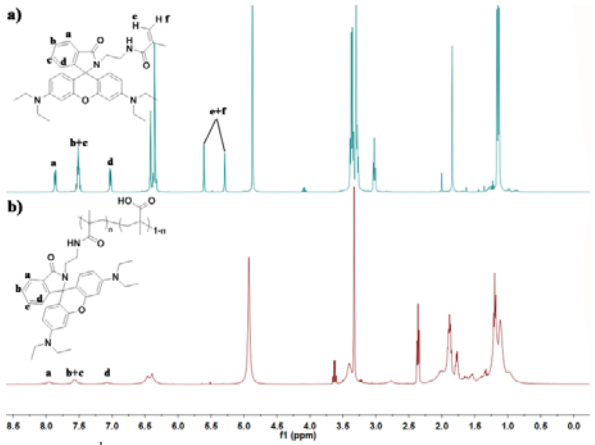

Fig. 2 ^{1}H-NMR spectra recorded for a) **M-2**, b) **P-2**. (in CD_3OD)

M-1, 5.78 ppm and 5.31 ppm for **M-2** were disappeared in the spectra of **P-1** and **P-2**. The three characteristic peaks of hydrogen atoms of rhodamine were still existed but we could found that the strength of signal became weaker due to the low rhodamine content in the polymer. To further determine the content of rhodamine, UV-vis absorption spectrum was introduced[53]. We prepared ethanol solutions of the two monomers with different concentrations, and obtained two concentration-based standard curves by detecting the absorbance of each concentration of the two monomers, respectively (Fig. S1). Then we measured absorbance of **P-1** and **P-2** (concentrations: 0.2 mg/ml in ethanol) and substituted the data of the two polymers in their standard curves, at last the concentrations of rhodamine group (C_{MR}) of the two polymers could be calculated. The rhodamine content of **P-1** and **P-2** were calculated to be 7.79% and 6.76%. And the diameter sizes of **P-1** and **P-2** were shown to be about 100 nm to 250 nm as determined by dynamic light scattering (Table S2), indicating that the as-prepared polymers readily self-assembled into polymeric nanoparticles upon sonication, and could enter the cell through endocytosis.

3.2 Fluorescence spectra properties of M-1, M-2, P-1 and P-2

It is imperative that the fluorescence intensity of probes could be enhanced while maintaining stringent selectivity for lysosomal pH. To make sure the polymer **P-1** and **P-2** could exhibit better application, their monomers **M-1** and **M-2** were firstly analyzed by fluorometry for their pH responsive characteristics.

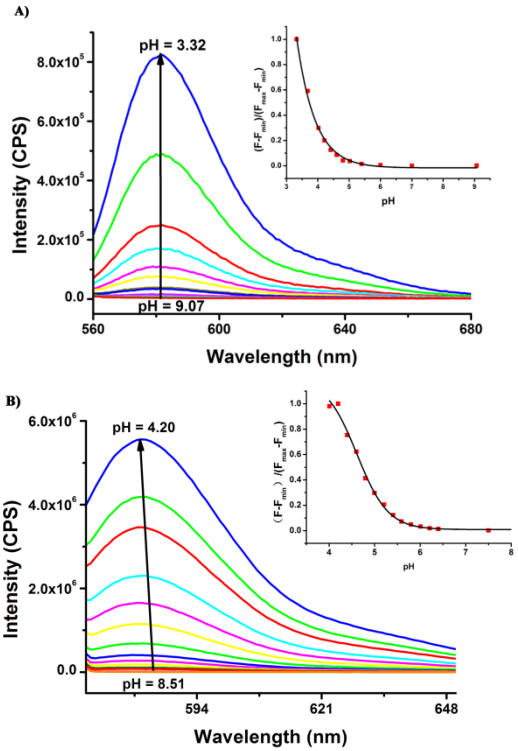

Fig. 3 A) Fluorescence spectral changes (λ_{ex} = 550 nm) of **M-1** (10 μM) in B-R buffer solution at different pH values, and maximum emission intensity was measured at 582 nm. Inset: Normalized fluorescence intensity as a function of pH for **M-1**. pH 3.32, 3.68, 4.02, 4.21, 4.41, 4.60, 4.80, 5.02, 5.28, 5.40, 5.61, 5.80, 6.00, 6.23, 6.41, 6.61, 6.80, 7.00, 7.54, 8.35, 9.07. B) Fluorescence spectral changes (λ_{ex} = 555 nm) of **M-2** (10 μM) in B-R buffer solution at different pH values, and maximum emission intensity was measured at 582 nm. Inset: Normalized fluorescence intensity as a function of pH for **M-2**.pH 4.20, 4.40, 4.60, 4.80, 5.00, 5.21, 5.41, 5.59, 5.80, 6.01, 6.21, 6.40, 7.50, 8.51.

The fluorescence pH titrations of **M-1** and **M-2** are displayed in Fig. 3, **M-1** and **M-2** are almost non-fluorescence at weak acidic pH (≈ pH 6.0), while with the pH decreasing, the fluorescence intensity at 582 nm of the two monomers gradually increased: **M-1** increased about 92–fold from pH 6.0 to 3.32; and **M-2** increased about 53–fold from pH 6.40 to 4.40. These results demonstrated that the ring-opening progress induced by H^+ still work. According to the study of J. W. Aylott that pK_a is generally the pH at which the fluorophore shows half its maximal response[54], the pK_a value of **M-1** and **M-2** was calculated as 3.37 and 4.71. As we have mentioned before, the pH scale of those acidic compartments (endosome and lysosome) and tumor tissue *in vivo* commonly in ranges from 4.5 to 6.0 and 6.2 to 6.9, respectively. The pK_a value of **M-1** is too acidic for lysosome, while **M-2** is more suitable. Moreover, the quantum yield of the two monomers are connected to pH values, it was determined to be 0.021, 0.229 under acidic condition (pH = 5.0) and 0.005, 0.007 at neutral pH values (pH = 7.0) for **M-1** and **M-2**,

respectively.

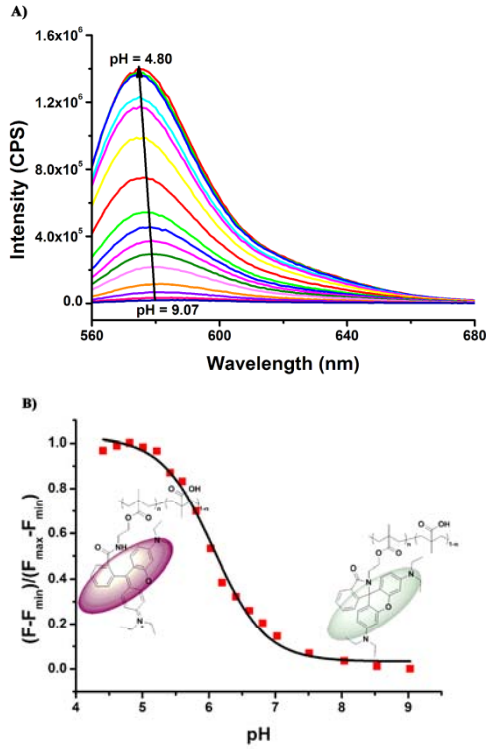

Fig. 4 A) Fluorescence spectral changes (λ_{ex} = 550 nm) of **P-1** (100 μg/ml) in B-R buffer solution at different pH values, and maximum emission intensity was measured at 582 nm. B) Normalized fluorescence intensity as a function of pH for **P-1**.pH 4.41, 4.60, 4.80, 5.02, 5.28, 5.40, 5.61, 5.80, 6.00, 6.23, 6.41, 6.61, 6.80, 7.00, 7.54, 8.04, 8.53, 9.07.

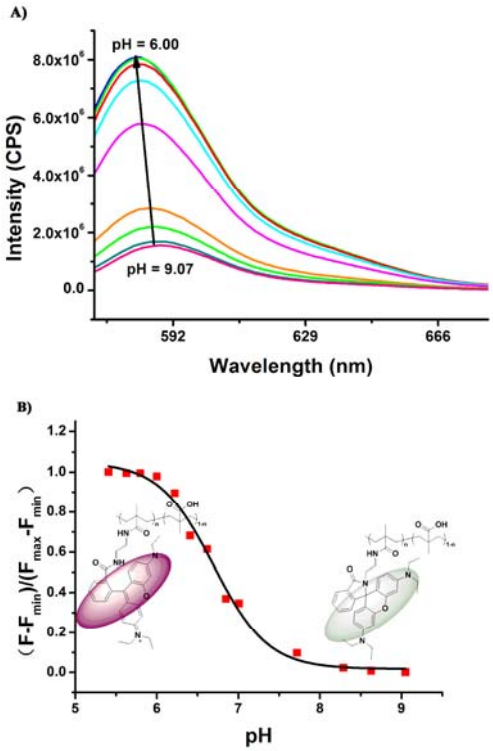

Fig. 5 A) Fluorescence spectral changes (λ_{ex} = 555 nm) of **P-2** (100 μg/ml) in B-R buffer solution at different pH values, and maximum emission intensity was measured at 582 nm. B) Normalized fluorescence intensity as a function of pH for **P-2**.pH 5.41, 5.63, 5.80, 6.00, 6.22, 6.41, 6.62, 6.85, 7.01, 7.72, 8.29, 8.63, 9.07.

Proton triggered fluorescence emission spectra of **P-1** and **P-2** are shown in Fig.4 and Fig.5. Although the content of rhodamine in the polymer is not very high, the fluorescence intensity of the polymer is good enough. Compared to the monomers **M-1** and **M-2**, the quantum yield of **P-1** and **P-2** were much higher: 0.364 for **P-1** and 0.439 for **P-2** (both calculated at neutral pH value) respectively. The trend of fluorescence intensity to pH values are identical to that of monomers, indicating that acid mediated opening of rhodamines pirolactam still works. For **P-1**, the fluorescence emission peak at 582 nm increased dramatically as the pH decreased from 7.0 to 5.5(Fig. 4), and the fluorescence emission peak at 582 nm of **P-2** also increased dramatically as the pH decreased from 7.5 to 6.0 (Fig. 5). These results suggested the high sensitivity of afore mentioned polymers. The pK_a for **P-1** and **P-2** were calculated as 6.07 and 6.71, which indicated its potential application for the imaging of acidic organelles and tumor tissue.

As known to all, the intracellular environment is really complicated and it contains different metal ions, such as K^+, Na^+, Ca^{2+}, Mg^{2+}, Cu^{2+}, Zn^{2+} and Fe^{3+}. Some of the metal ions might bind with the amido bond of our probes and thus interfere in the proton triggered ring-opening reaction of the probes.[17] In order to confirm the selectivity and reliability of **M-1**, **M-2**, **P-1** and **P-2,** fluorescence

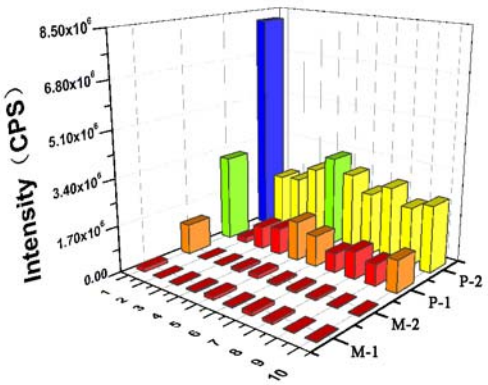

Fig. 6 Selectivity of **M-1**, **M-2**, **P-1** and **P-2** for pH over selected interferences in B-R buffer solution (pH 7.5). The concentration of each compound: 10 μM for **M-1** and **M-2**,100 μg/ml for **P-1** and **P-2**. Different ions from 1 to 10: H^+, OH^-, Na^+, K^+, Ca^{2+}, Co^{2+}, Cu^{2+}, Zn^{2+}, Fe^{3+}, Mn^{2+}, Mg^{2+}(the concentration of metal ions: 2 mM)

emission spectrometry was studied. As shown in Fig. 6, contrasting the selectivity of the two monomers, we could find that **M-2** was more suitable for indicating pH variations. However, it should be noted that **M-1** and **M-2** exhibited poor water solubility during the whole fluorescence property studies. The poor solubility limits the application of them. Therefore, rhodamine based polymers with suitable water solubility were prepared to overcome that obstacle. After copolymerized with methacrylic acid, the water solubility of **P-1** and **P-2** were improved greatly. Meanwhile, the fluorescence intensity of **P-1** and **P-2** were much higher than **M-1** and **M-2** even at lower concentration. Moreover, although the selectivity of **P-1** and **P-2**

were almost the same, the fluorescence intensity of **P-2** was much higher than that of **P-2** at the same pH, which means **P-2** would be much more appropriate in intracellular imaging. In short, the high sensitivity of **M-2**, **P-1**, **P-2** to proton and their high selectivity over interfering species demonstrates that all of these three compounds have a potential for applications in lysosomes-specific imaging *in vivo* cells.

3.3 Lysosome-specific fluorescence imaging in living cells

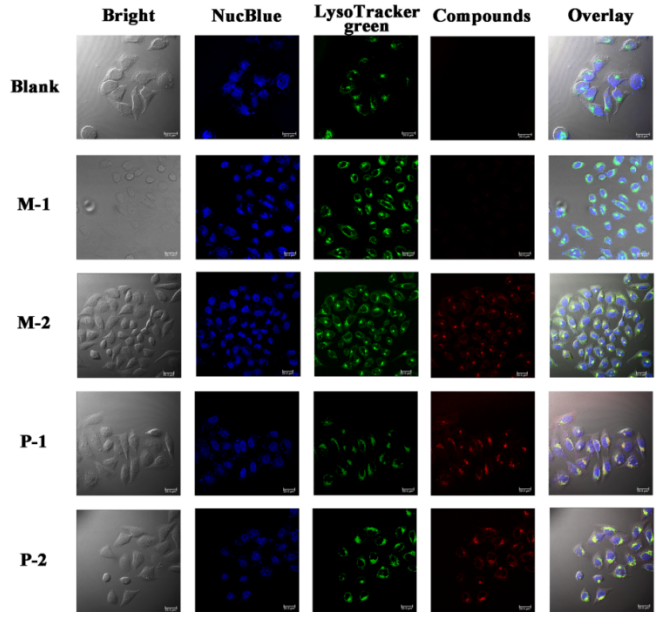

Fig. 7 Confocal microscopy images of the intracellular distribution of lysosomes (incubation 30 min). Rows: "Blank"-Hela cells incubated with NucBlue (one drop per milliliter) and LysoTracker Green (1 μM) as control; "**M-1**"-Hela cells was stained with5 μM **M-1**(red channel), 1 μM LysoTracker Green (green channel) and one drop NucBlue (blue channel); "**M-2**"-Hela cells was stained with5 μM **M-2** (red channel), 1μM LysoTracker Green (green channel) and one drop NucBlue (blue channel); "**P-1**"-Hela cells was stained with 25 μg/ml **P-1** (red channel), 1μM LysoTracker Green (green channel) and one drop NucBlue (blue channel); "**P-2**"-Hela cells was stained with 25 μg/ml **P-2** (red channel), 1μM LysoTracker Green (green channel) and one drop NucBlue (blue channel). Blue channel: λ_{ex} = 405 nm, λ_{em} = 420 ~ 470 nm; green channel: λ_{ex} = 488 nm, λ_{em} = 500 ~ 540 nm; red channel: λ_{ex} = 552 nm, λ_{em} = 565 ~ 620nm.

P-1 and **P-2** exhibited outstanding sensitivities to pH, and then the imaging and sensing of the pH *in vivo* cells were studied by confocal laser scanning microscopy analysis. Hela cells were used to further investigate the localization of **M-1**, **M-2**, **P-1** and **P-2**, and concentration of **M-1**, **M-2** and **P-1**, **P-2** were 5 μM and 25 μg/ml, respectively. To confirm the probes could located lysosomes, Hela cells were co-stained with commercially available nucleus-specific and lysosome-specific staining probe, NucBlue® Live Cell Stain (one drop per milliliter) and Lysotracker green DND-26 (1 μM). As shown in Fig. 7, Hela cells only co-stained with NucBlue and LysoTracker green does not give off any light under the excitation of 552 nm, but the cells stained with **M-1** emitted extremely weak red fluorescence, and **M-2**, **P-1, P-2** emitted bright red emission distributed mainly in the cytoplasm with the excitation of 552 nm. This also confirmed by only minimal colocalization of the red emissions of **M-1**, **M-2**, **P-1** and **P-2** with blue emission from nucleus-specific NucBlue.

The orange fluorescence of overlay also illustrated the same subcellular localization of LysoTracker green with **M-2**, **P-1** and **P-2**. In order to substantiate whether these compounds really can be used for lysosome (acidic compartment) specific staining, a qualitative colocalization index was measured by choosing a

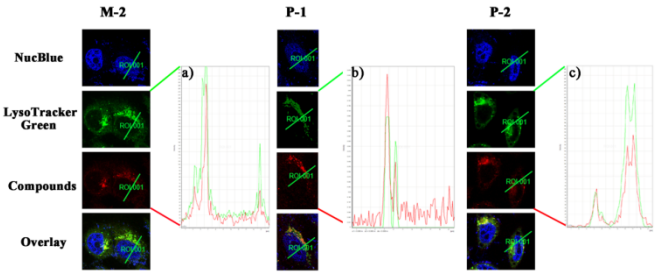

Fig. 8 Columns: **M-2**- confocal microscopy images of Hela cells co-stained with 5 μM **M-2**, 1 μM LysoTracker Green and one drop NucBlue; **P-1**- confocal microscopy images of Hela cells co-stained with 25 μg/ml **P-1**, 1 μM LysoTracker Green and one drop NucBlue; **P-2**- confocal microscopy images Hela cells co-stained with 25 μg/ml **P-2**, 1 μM LysoTracker Green and one drop NucBlue. a) ~ c): Intensity profile of regions of interest (ROI) across Hela cells.

Region of Interest (ROI) in one cell (Fig.8). The green line means the signal of LysoTracker Green from the region we chose and the red line means the signal of **M-2**, **P-1** or **P-2** from the same region. The three coordinate graphs in Fig. 8 illustrated that no matter the green line or the red line the peaks were all in the same position, proving that **M-2**, **P-1** and **P-2** indeed located in lysosomes. Furthermore, the cytotoxicities of **P-1** and **P-2** were also detected, and the result indicated no obvious toxicities were found for the two polymers in cells even at the concentration of 500 μg/ml (Fig.9). However, due to the poor water solubility of **M-1** and **M-2**, their cytotoxicities were not achieved.

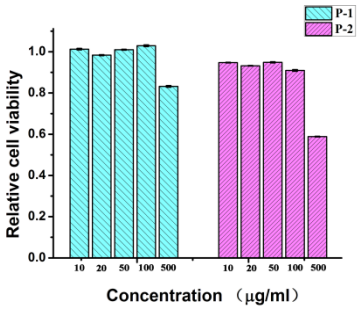

Fig. 9 Cytotoxicity of **P-1** and **P-2** on Hela cells.

3.4 Zebrafish and nude mice imaging

To further explore the application of Rhodamine-based polymers, fluorescence imaging in animal models was conducted. Considering zebrafish that has high homology with mammals is optically transparent during early development[55], confocal laser scanning micrographs of zebrafish was taken. The variation of pH inside zebrafish was influenced by the external environment, thus we washed zebrafish with pH 5.0 and pH 7.0 PBS (10 mM) for 5 min respectively to remove disturbances. As shown in Fig.10 and Fig. 11, no fluorescence was observed in the absence of probes. When zebrafish incubated with **M-1** and **M-2,** also no fluorescence was found, no matter zebrafish under what condition (pH 5.0 or pH 7.0). This is because the poor solubility of **M-1** and **M-2,** which make it hard to entry into the zebrafish. However,

once the zebrafish incubated with **P-1** and **P-2** at the same conditions**,** bright red emission was observed only under acidic condition (pH = 5.0), which indicated the opening of rhodamines pirolactam. These results indicated: a) the polymers had more advantages in bio-imaging than **M-1** and **M-2**; b) **P-1** and **P-2**

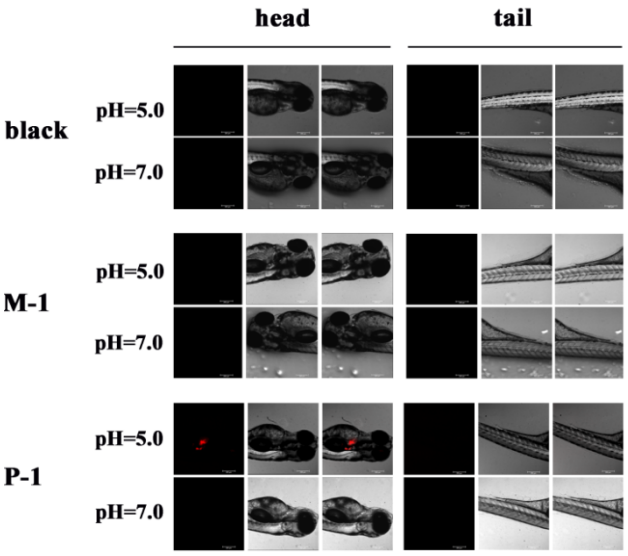

Fig. 10 Confocal laser fluorescence microscopy images of zebrafish. The zerbrafish incubated with the same compound and then washed with pH 5.0 and pH 7.0 PBS (10 mM), respectively. The zebrefish were devided into six groups and every two groups incubated with none, **M-1** (100 μM) and **P-1** (500 μg/ml), respectively. (λ_{ex} = 552 nm, λ_{em} = 565 ~ 620nm.)

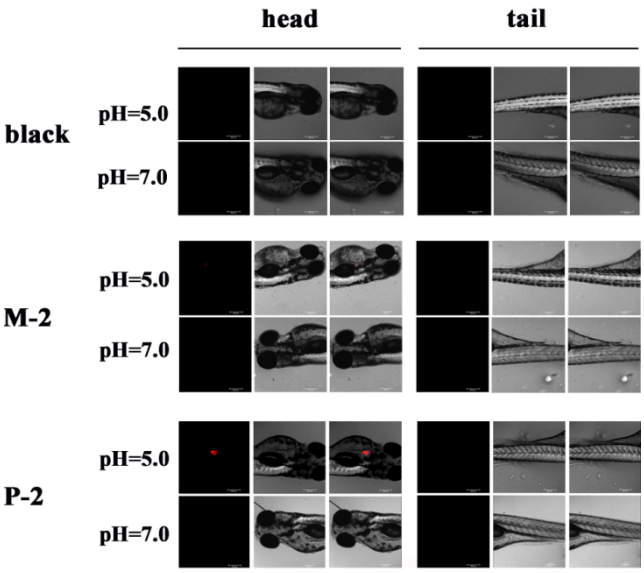

Fig. 11 Confocal laser fluorescence microscopy images of zebrafish. The zebrefish were devided into six groups and every two groups incubated with none, **M-2** (100 μM) and **P-2** (500 μg/ml), respectively. The zerbrafish incubated with the same compound and then washed with pH 5.0 and pH 7.0 PBS (10 mM), respectively. (λ_{ex} = 552 nm, λ_{em} = 565 ~ 620nm.)

could enrich in liver of zebrafish through the digestive system rather than the whole body, and this phenomenon hold great promise for visual treating liver-related disease; c) **P-1** and **P-2** had liver-enrichment only under acidic environment (pH = 5.0) also indicated that these polymer had the potency for the diagnosis of cancer and the excision of tumor tissue. Additionally, zebrafish remained viable throughout the whole experiments (3- 4 h), elucidated the low toxicity of **P-1** and **P-2**.

Finally, considering **M-1** and **M-2** had non-fluorescence in zebrafish under acidic condition, we only studied fluorescence imaging of **P-1** and **P-2** in nude mice (Fig.12). Firstly, **P-1** and **P-2** in different pH PBS buffer solution (pH 5.0, pH 7.0) was prepared, then exposed the mouse to skin injections of **P-1** and **P-2**. We could find from Fig.12 that under acidic environment, **P-1** and **P-2** both given out light but the light emitted from **P-1**was much more weaker, and only **P-2** given out weak light under neutral condition. We demonstrated that rhodamine-based compound could really be used for vivo imaging, and contrasted **P-1** with **P-2**, the imaging result of **P-2** is much better which may due to that under complex vivo condition amide bond is more stable than the ester bond. As we expected, **P-1** and **P-2** had the potency for the visualization of cancerous tissue *in vivo* by sensing the tumor acidic microenvironments.

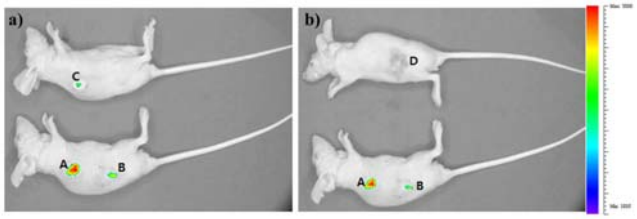

Fig. 12 The fluorescent imaging of nude mice. a) A: **P-2**200 μl 10 mg/ml pH 5.0, B: **P-2** 200μl 10 mg/ml pH 7.0, C: **P-1** 200 μl10 mg/ml pH 5.0; b) A: **P-2** 200 μl 10 mg/ml pH 5.0, B: **P-2** 200μl 10 mg/ml pH 7.0, D: **P-1** 200μl 10 mg/ml pH 7.0. (λ_{ex} = 534 nm)

Conclusions

In summary, we have designed two different rhodamine-based polymer probes (**P-1** and **P-2**) with remarkable pH sensitivity, which could locate in lysosomes. The polymers could be synthesized by simple free radical polymerization and form into nanoparticles in water solution with the diameter from 100 nm to 250 nm at different concentrations. Compared with their monomer **M-1** and **M-2**, the water solubility of polymers increased visibly and the fluorescence intensity was enhanced obviously at acid condition, revealed that they are suitable for imaging in intracellular acidic organelles. As expected, **P-1** and **P-2** exhibited bright red emission only in the lysosomes with low cytotoxicity. The confocal laser scanning micrographs imaging of zebrafish also showed that **P-1** and **P-2** could enrich in liver and only give off red emission under acid condition, which indicated that these two probes have potential applications for labeling liver-related medicines and tracing disease. Moreover, the fluorescence imaging of nude illustrated the potency for the visualization of cancerous tissue *in vivo* by sensing the tumor acidic microenvironments.

Acknowledgments

This work was financially supported by the National Program on Key Basic Research Project of China (973 Program, 2012CB720603 and 2013CB328900), the National Science

Foundation of China (Nos. 21232005, 21321061, J1310008 and J1103315), and the Specialized Research Fund for the Doctoral Program of Higher Education in China (20120181130006). We also thank the Analytical & Testing Center of Sichuan University for NMR analysis.

Notes and references

[a] *Key Laboratory of Green Chemistry and Technology (Ministry of Education), College of Chemistry, Sichuan University, Chengdu, 610064, China Fax: (86)-28-85415886 ; Tel: (86)-28-85415886; E-mail: kli@scu.edu.cn; xqyu@scu.edu.cn.*

[b] *State Key Laboratory of Biotherapy, West China Hospital, West China Medical School, Sichuan University, Chengdu 610041, China E-mail: xieym@scu.edu.cn*

† Electronic Supplementary Information (ESI) available. [GPC data, dynamic light scattering results and spectra of compounnds] See DOI: 10.1039/b000000x/

1 J. R. Casey, S. Grinstein and J. Orowski, *Nat. Rev. Mol. Cell Biol*., 2010, **11**, 50-61;
2 J. Y. Han and K. Burgess, *Chem. Rev.*, 2010, **110**, 2790-2728;
3 Z. Li, S. Q. Wu, J. H. Han, L. Yang and S. F. Han, *Talanta*, 2013, **114**, 254-260;
4 B. Turk and V. J. Turk, *Biol. Chem.*, 2009, **284**, 21783-21787;
5 R.Wang, C. W. Yu, F. B. Yu and L. X.Chen, *Trends Anal. Chem.*, 2010, **29**, 1004-1013;
6 R. Pal and D. Parker, *Chem. Commun.*, 2007, **5**, 474-476;
7 K. M. Sun, C. K. McLaughlin, D. R. Lantero and R. A. Manderville, *J. Am. Chem. Soc.*, 2007, **129**, 1894-1895;
8 H. M. Kim, M. J. An, J. H. Hong, B. H. Jeong, O. Kwon, J. Y. Hyon, et al. *Angew. Chem. Int. Ed.*, 2008, **47**, 2231-2234;
9 J. M. Hu, X. Z. Zhang, D. Wang, X. L. Hu, T. Liu, G. Y. Zhang, et al. *J. Mater. Chem.*, 2011, **21**, 19030-19038;
10 Z. Li, S. Q. Wu, J. H. Han and S. F. Han, *Analyst*, 2011, **136**, 3698-3706;
11 H. S. Lv, S. Y. Huang, B. X. Zhao and J. Y. Miao, *Anal. Chim. Acta*, 2013, **788**, 177-182;
12 W. S. Zhang, B. Tang, X. Liu, Y. Y. Liu, K. H. Xu, J. Q. Ma, et al. *Analyst*, 2009, **134**, 367-371;
13 H. Zhu, J. L. Fan, Q. L. Xu, H. L. Li, J. Y. Wang, P. Gao, et al. *Chem. Commun.*, 2012, **48**, 11766–11768;
14 J. Stinchcombe, G. Bossi and G. M. Griffiths, *Science*, 2004, **305**, 55-59;
15 X. J. Wan and S. Y. Liu, *J. Mater. Chem.*, 2011, **21**, 10321-10329;
16 K. J. Zhou, H. M. Liu, S. R. Zhang, X. N. Huang, Y. G. Wang, G. Huang, et al. *J. Am. Chem. Soc.*, 2012, **134**, 7803-7811;
17 H. S. Lv, J. Liu, J. Zhao, B. X. Zhao and J. Y Miao,. *Sensors Actuat B*, 2013, **177**, 956-963;
18 Z. Q. Hu, M. Li, M. D. Liu, W. M. Zhuang and G. K. Li, *Dyes Pigments*, 2013, **96**, 71-75;
19 Y. M. Yang, Q. Zhao, W. Feng and F. Y. Li, *Chem. Rev.*, 2013, **113**, 192–270;
20 C. J. Zhou, Y. J. Li, Y. J. Zhao, J. H. Zhang, W. L. Yang and Y. L. Li, *Org. Lett.*, 2011, **13**, 292-295;
21 E. Kim, S. H. Lee and S. B. Park, *Chem. Comm.*, 2011, **47**, 7734-7736;
22 X. L. Zhang, Y. Jiao, X. Jing, H. M. Wu, G. J. He and C. Y. Duan, *Dalton Trans.*, 2011, **40**, 2522-2527,
23 T. Jokic, S. M. Borisov, R. Saf, D. A. Nielsen, M.Kühl and I. Klimant, *Anal. Chem.*, 2012, **84**, 6723-6730;
24 R. Tang, H. Lee and S. J. Achiefu, *Am. Chem. Soc.*, 2012, **134**, 4545-4548;
25 S. J. Chen, J. Z. Liu, Y. Liu, H. M. Su, Y. N. Hong, C. K. W. Jim, et al. *Chem. Sci.*, 2012, **3**, 1804-1809;
26 L. Yuan, W. Y. Lin, Z. M. Cao, J. L. Wang and B. Chen, *Chem.-Eur. J.*, 2012, **18**, 1247-1255;
27 S. S. Zhu, W. Y. Lin and L. Yuan, *Dyes Pigments*, 2013, **99**, 465-471;
28 W. M. Huang, W. Y. Lin and X. Y. Guan, *Tetrahedron Lett.*, 2014, **55**, 116-119;
29 M. Tantama, Y. P. Hung and G. J. Yellen, *Am. Chem. Soc.*, 2011, **133**, 10034-10037;
30 X. Z. Yan, F. Wang, B. Zheng and F. H. Huang, *Chem. Soc. Rev.*, 2012, **41**, 6042-6065;
31 A. M. Breul, M. D. Hager and U. S. Schubert, *Chem. Soc. Rev.*, 2013, **42**, 5366-5407;
32 L. Albertazzi, B. Storti, L. Marchetti and F. Beltram, *J. Am. Chem. Soc.*, 2010; **132**, 18158-18167;
33 C. Li, K. Li, H. H. Yan, G. H. Li, J. S. Xia and X. B. Wei, *Chem. Commun.*, 2010, **46**, 1326–1328;
34 W. Shi, X. H. Li and H. M. Ma, *Angew. Chem. Int. Ed.*, 2012, **51**, 6432-6435;
35 S. Chang, X. M. Wu, Y. S. Li, D. Niu, Y. P. Gao, Z. Ma, et al. *Biomaterials*, 2013, **34**, 10182-10190;
36 Z. Li, Y. L. Song, Y. H. Yang, L. Yang, X. H. Huang, J. H. Han, et al. *Chem. Sci.*, 2012, **3**, 2941-2948;
37 X. J. Wu, Y. P. Tian, M. Z. Yu, J. H. Han and S. F. Han, *Biomater. Sci.*, 2014, DOI: 10.1039/c4bm00007b;
38 S. Dai, P. Ravi and K. C. Tam, *Soft Matte*, 2008, **4**, 435–449;
39 W. W. He, H. J. Jiang, L. F. Zhang, Z. P. Cheng and X. L. Zhu. *Polym. Chem.*, 2013, **4**, 2919-2938;
40 L. J. Bai, L. F. Zhang, Z. P. Cheng and X. L. Zhu, *Polym. Chem.*, 2012, **3**, 2685–2697.
41 M. Beija, C. A. M. Afonso and J. M. G. Martinho, *Chem. Soc. Rev.*, 2009, **38**, 2410-2433;
42 H. N. Kim, M. H. Lee, H. J. Kim, J. S. Kim and J. Yoon, *Chem. Soc. Rev.*, 2008, **37**, 1465–1472;
43 X. Q. Chen, T. Pradhan, F. Wang, J. S. Kim and J. Yoon, *Chem. Rev.*, 2012, **112**, 1910–1956
44 L. Yuan, W. Y. Lin, K. B. Zheng and S. S. Zhu, *Acc. Chem. Res.*, 2013, **46**, 1462–1473;
45 L. Yuan. W. Y. Lin, Y. N. Xie, B. Chen and S. S. Zhu, *J. Am. Chem. Soc.*, 2012, 134, 1305–1315;
46 L. Yuan, W. Y. Lin, Y. N. Xie, B. Chen and J. Z. Song, *Chem.-Eur. J.*, 2012, **18**, 2700-2706;
47 L. Yuan, W. Y. Lin, Y. N. Xie, S. S. Zhu and S. Zhao, *Chem.-Eur. J.*, 2012, **18**, 14520-14526;
48 H. B. Yu, Y. Xiao and L. J. Jin, *J. Am. Chem. Soc.*, 2012, **134**, 17486−17489;
49 T. Y. Liu, Z. C. Xu, D. R. Spring and J. G. Cui, *Org. Lett.*, 2013, **15**, 2310-2313;
50 H. J. Kim, C. H. Heo and H. M. Kim, *J. Am. Chem. Soc.*, 2013, **135**, 17969-17977;
51 M. Z. Tian, X. J. Peng, J. L. Fang, J. Y. Wang and S. G. Sun, *Dyes Pigments*, 2012, **95**, 112-115;
52 X. F. Zhou, F. Y. Su, H. G. Liu, P. S. Willis, Y. Q. Tian, R. H. Johnson, et al. *Biomaterials*, 2012, **33**, 171-180;
53 Y. Qi, N. Y. Li, Q. F. Xu, X. W. Xia, J. F. Ge and J. M. Lu, *React. Funct. Polym.*, 2011, **71**, 390-394;
54 V. M. Chauhan, G. R. Burnett and J. W. Aylott, *Analyst*, 2011, **136**, 1799-1801;
55 S. K. Ko, X. Q. Chen and J. Yoon, *Chem. Soc. Rev.*, 2010, **40**, 2120-2130.

